# Phase Behavior of Aqueous Mixtures of 2-Phenylbenzimidazole-5-sulfonic Acid and Cetyltrimethylammonium Bromide: Hydrogels, Vesicles, Tubules, and Ribbons

**D. Gräbner,[†] L. Zhai,[‡] Y. Talmon,[§] J. Schmidt,[§] N. Freiberger,[||] O. Glatter,[||] B. Herzog,[⊥] and H. Hoffmann*,[†]**

*BZKG, University of Bayreuth, Gottlieb-Keim-Strasse 60, 95448 Bayreuth, Germany, College of Chemistry and Chemical Engineering, Jinan University, 106 Jiwei Road, Jinan 250022, People's Republic of China, Department of Chemical Engineering, Technion—Israel Institute of Technology, Haifa, Israel 32000, Institut für Physikalische Chemie, University of Graz, Heinrichstrasse 28, A-8010 Graz, Austria, and Ciba Spezialitätenchemie Grenzach GmbH, P.O. Box 12 66, 79630 Grenzach-Wyhlen, Germany*

*Received: June 25, 2007; In Final Form: November 23, 2007*

We studied the phase behavior and aggregation in mixed aqueous solutions of the anionic UV-absorber 2-phenylbenzimidazole-5-sulfonic acid sodium salt, PhBSA (Na salt), and the cationic surfactant cetyltrimethylammonium bromide, CTAB. The mixtures of the two components behave similarly to catanionic surfactant mixtures. The samples on the PhBSA-rich side have low viscosity and are turbid. The turbidity, due to uni- and multilamellar vesicles (SUVs and MLVs), increases with the mole ratio of CTAB. The interbilayer distance inside the MLV changes with the mole ratio of the two components from a few 10 nm for the 7:3 (molar ratio of PhBSA, Na salt, to CTAB) system to practically zero for the 5:5 mixture. The latter mixture forms a precipitate within less than 1 h. With the exception of the 5:5 mixture, all samples on the PhBSA-rich side are stable for many days. After that period, within one more day, the turbid vesicle phases are transformed into more or less clear hydrogels. We found that the gelation is due to the formation of very long stiff tubules about 14 nm in diameter, which is independent of the mixing ratio of the samples. The hydrogels and the tubules melt around 45 °C. On the CTAB-rich side, the 4:6 sample behaves like the 6:4 sample, whereas at 3:7 a precipitate was found to form shortly after mixing. At still smaller PhBSA (Na salt) to CTAB ratios, only clear, viscoelastic solutions are found that do not change with time. We determined the micellar structures in the samples by cryo-TEM and by SAXS. The rheological properties of the hydrogels and of the viscoelastic samples were characterized by oscillating rheological measurements. DSC measurements indicated that the tubules are in a semicrystalline state and melt at around 45 °C. The semicrystalline bilayer of the tubules seems to have a 1:1 composition of PhBSA to CTAB. The excess PhBSA seems to be adsorbed on the tubules. It is assumed that the stiffness of the bilayer of the vesicles and the stiffness of the tubules are due to the stiffness of the PhBSA molecule.

## Introduction

Carbon nanotubes (NTs) are most interesting structures in nanotechnology.[1] They have a high potential for various applications in nanotechnology. The smallest and the most stable NTs are the single-wall carbon nanotubes (SWNTs).[2] They are now commercially available and are tested for various applications such as incorporation in polymers to strengthen their mechanical properties. Because of their electric conductivity, they can also be used for batteries and fuel cells.

Another route to nanotubes of small diameters is by self-aggregation of a number of lipid molecules.[3] NTs have been found with zwitterionic phospholipids,[4] with cationic,[5] nonionic,[6] and anionic[7] surfactant solutions. NTs have also been found in double-chain ionic surfactant solutions.[8] They usually occur in situations in which bilayer-type aggregates, such as vesicles or disclike micelles, can be observed. According to our knowledge, all the reported tubules were observed in binary systems where only one phospholipid compound was dispersed in water.

Recently, however, we have observed NTs when aqueous solutions of a cationic surfactant were mixed with a rigid, negatively charged, amphiphilic molecule.[9] These tubules had a small outer diameter of only 12 ± 1 nm and were extremely stiff. Their persistence length was more than 1 $\mu$m. Only preliminary information on the novel NTs was given.[9] In particular, we reported only the processes and the structures that occurred when solutions with an excess of the stiff anionic molecule 2-phenylbenzimidazole-5-sulfonic acid (PhBSA) as the Na salt were mixed with the cationic surfactant *N*-hexadecyl-*N*,*N*,*N*-trimethylammonium bromide (CTAB). In this paper, the whole mixing range from the soluble pure compound (Na salt) to the pure CTAB is covered.

As was shown with other catanionic systems, several structures are observed as a function of the mole ratio of the two components.[10−13] In particular, we emphasize the hydrogels that are observed on the PhBSA-rich side of the phase diagram of the two components.

* To whom correspondence should be addressed. Phone: +49-921-50736-135. Fax: +49-921-50736-139. E-mail: heinz.hoffmann@nmbgmbh.de, heinz.hoffmann@uni-bayreuth.de.
[†] University of Bayreuth.
[‡] Jinan University.
[§] Technion—Israel Institute of Technology.
[||] University of Graz.
[⊥] Ciba Spezialitätenchemie Grenzach GmbH.

10.1021/jp0749423 CCC: $40.75 
Published on Web 02/15/2008

## Materials and Methods

**Cryo Transmission Electron Microscopy (Cryo-TEM)**. Vitrified specimens for cryo-TEM were prepared in a controlled environment vitrification system (CEVS) and quenched into liquid ethane at its freezing point. Details are given elsewhere.[14] Specimens, kept below −178 °C, were examined in an FEI TI2 $G^2$ transmission electron microscope, operated at 120 kV, using a Gatan 626 cryoholder system. Images were recorded digitally in the minimal electron dose mode by a Gatan US1000 high-resolution CCD camera with the Digital Micrograph software package.

**Differential Scanning Calorimetry (DSC)**. The measurements were performed by a Setaram MikroDSC III in screw-capped stainless steel cells holding ca. 850 $\mu$L. The sample mass was ca. 500 mg. The reference container was filled with ca. 500 mg of deionized water. The samples were heated from 25 to 80 °C and cooled again to 25 °C; this cycle was performed three times to check reversibility of the transitions. The heating-to-cooling rate was 0.5 K/min. At 25 °C, the samples were kept isothermal for 60 min; at 80 °C, this period, for technical reasons, was only 20 min.

**Rheological Measurements**. The rheological measurements were performed by a Haake RS 600 apparatus with a cone and plate sensor and a Haake RS 300 with a double-gap cylinder sensor. The sensor systems were chosen according to the fluidity of the sample: RS 600 for highly viscous liquids and RS 300 for low-viscosity liquids (<100 mPa·s). Temperature in the measuring system was controlled to ±0.1 °C by a thermocontroller (Haake TC 81) for the RS 600 and by an ethylene glycol circulator, ThermoHaake DC30/K20, with an accuracy of ±0.5 °C for the RS 300. The viscous properties were determined by steady-state shear rate ramping and the viscoelastic properties by oscillatory measurements from 0.01 to 10 Hz, for which the deformation was controlled in the linear region.

**Small-Angle X-ray Scattering (SAXS)**. The SAXS equipment consisted of a SAXSess camera (Anton-Paar, Graz, Austria) connected to an X-ray generator (Philips, PW 1730/10) operating at 40 kV and 50 mA, with a sealed-tube Cu anode. A Göbel mirror was used to convert the divergent polychromatic X-ray beam into a focused line-shaped beam of Cu Kα radiation ($\lambda = 0.154$ nm). The 2D scattering pattern was recorded by a PI-SCX fused fiber optic taper CCD camera from Princeton Instruments, which is a division of Roper Scientific, Inc. (Trenton, NJ). The used CCD detector features a 2084 × 2084 array with a 24 × 24 $\mu$m pixel size (chip size 50 × 50 mm). The CCD is operated at −30 °C with 10 °C water-assisted cooling to reduce the thermally generated charge. Cosmic ray correction and background subtraction were performed on the 2D image before further data processing. The 2D image was integrated into the one-dimensional scattering function $I(q)$ using SAXSQuant software (Anton-Paar), where $q$ is the length of the scattering vector, defined by $q = (4\pi/\lambda)\sin(\theta/2)$, $\lambda$ being the wavelength and $\theta$ the scattering angle. The camera volume was kept under vacuum during the measurements to minimize background scattering from air. The temperature was controlled and kept at 25 ± 0.1 °C by using a Peltier element. The sample holder was a 1 mm quartz capillary.

After subtraction of the solvent background, the scattering curves are corrected for instrumental broadening and transformed into real space using the indirect Fourier transformation (IFT) method.[15,16] In the case of elongated cylinders this results in the cross-section pair distance distribution function $p_c(r)$.[17]

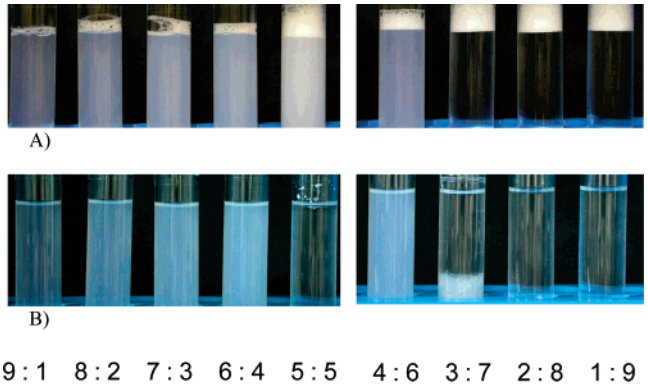


**Figure 1.** Samples of mixtures of PhBSA (Na salt) with CTAB for different mole ratios. The total concentration, $c°$, of the two components is 20 mM. $T = 25$ °C. (A) Freshly prepared; note the foam on top of the samples. (B) Two weeks after mixing. The sample with the mole ratio 5:5 contains a precipitate at the bottom of the test tube. Note that the first four samples on the left side are more transparent than in (A).

This function can finally be deconvoluted into the radial difference (relative to the solvent) electron density distribution $\Delta\rho(r)$.[18,19]

## Results and Discussion

**Phase Behavior**. Both components form transparent, optically isotropic low-viscosity solutions in water above 25 °C. When solutions of the two components are mixed, one obtains immediately optically isotropic, low-viscosity and turbid solutions. Note: Molar ratios always first give the fraction of PhBSA (Na salt) and then the CTAB fraction, so 9:1, e.g., means 9 parts PhBSA (Na salt) and 1 part CTAB.

Photos of the samples of PhBSA (Na salt) and CTAB at different mixing molar ratios are shown in Figure 1A. The samples show that the turbidity increases from the 9:1 to the 5:5 mixture. The 5:5 sample forms a precipitate within a few minutes after mixing, and a sediment is visible at the bottom of the sample. This sample does not further change with time. The 4:6 sample is somewhat turbid, is stable for several days, and looks like the 6:4 sample, whereas the 3:7 sample forms a precipitate. The other three samples on the CTAB-rich side are transparent and viscous.

The results are an indication that large aggregates have been formed in all the mixtures, and these aggregates are responsible for the turbidity or the viscosity of the samples. The samples do not change for several days and seem to be stable. However, two weeks later the samples on the PhBSA-rich side look completely different. The exact time in which the samples did not change depended on the mixing ratio; it decreased with the increasing mole ratio of CTAB from 10 days to a few days. Then, within 1 day, the samples became more transparent and at the same time gelled. The gelled samples are shown in Figure 1B.

Even for a total concentration of only 10 mM the formed hydrogels are quite stiff; the samples can be turned upside down without noticeable flow. In the gelled state the samples are still optically isotropic. However, when the samples are tilted for a longer period of time, they begin to deform in an elastic, reversible way, causing stress birefringence, Figure 2A.

With increasing temperature the hydrogels are stable up to about 45 °C. Then they melt to a low-viscosity solution that has the same appearance as the solution before the gelation. The transition is thermoreversible. The turbid state can however be supercooled. A cylindrical piece of the hydrogel from the test tube is shown in Figure 2B. The gel can easily be taken

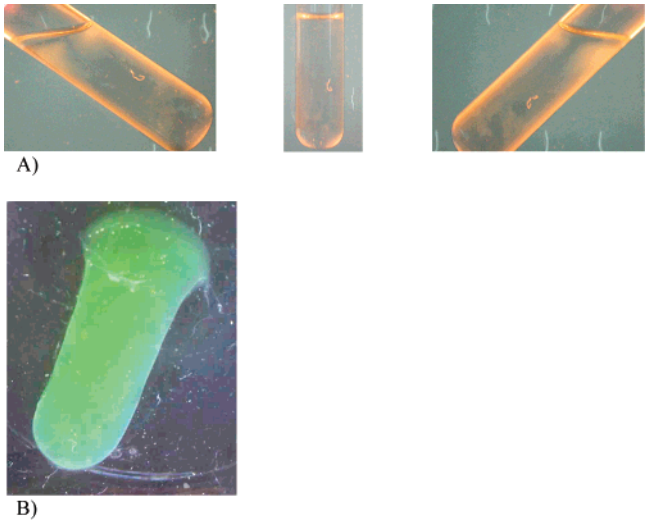

**Figure 2.** (A) Sample with a mole ratio of 8:2, $c^\circ = 10$ mM, after gelation, photographed between crossed polarizers. (B) A cylindrical piece of a sample with the same composition as in (A) in excess water, dyed with a water-soluble dye to enhance contrast.

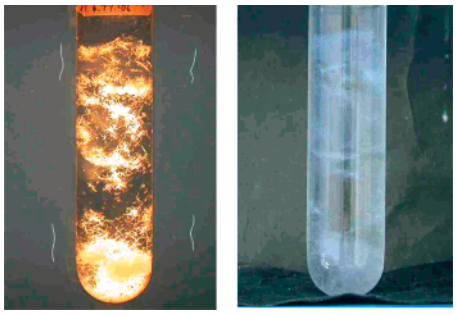

**Figure 3.** Sample with a mole ratio of 5.5:4.5, $c^\circ = 10$ mM, after several weeks, shown between crossed polarizers (left) and in direct light (right). Note small birefringent crystals trapped in the hydrogel.

out of the test tube by placing the test tube in hot water until the surface of the gel melts. It then slides out of the tube and can be placed in a larger tube. The gel does not change its shape for hours; only the upper part swells radially. As this top part was slightly sheared when the sample was tilted to check the sample gelation, the gelation process could have been disturbed, yielding a weaker gel in that part of the sample.

The gelled state of the samples is still not yet the thermodynamic equilibrium state. After several weeks white spots developed in the hydrogels; those became larger with time. They are most visible between crossed polarizers, because of their birefringence. In the PhBSA (Na salt)/CTAB system this crystalline state is most reproducibly formed at a composition of 5.5:4.5. In samples in which CTAB is replaced by $C_{18}$TAC, the crystalline state can be observed in all the PhBSA (Na salt)-rich systems. The crystals thus precipitate to the bottom of the test tube. A sample in which crystals are trapped in the hydrogel state is shown in Figure 3.

The observations described above indicate that the mixed solutions undergo three well-defined states with time: a turbid, low-viscosity state, A, the gelled state, B, and a crystalline state, C. When the chain length on the surfactant is changed in the mixtures, the situation remains more or less the same. The three states A, B, and C are observed at room temperature for $C_{18}$-TAC only. The $C_{16}$ and the $C_{14}$ systems show only the A and B states at room temperature, while the $C_{12}$ system goes directly into state C after mixing. It is likely, however, that the three states do occur in the latter systems when the temperature is lowered. The chain-length dependence of those states will be reported in a forthcoming paper.

**Cryo-TEM**. We applied cryo-TEM to examine the system at hand in two states: the turbid state (A) and the gelled state (B).

*Turbid State*. Figure 4A is a cryo-TEM micrograph of a vitrified specimen of a mixed sample with a total concentration of 10 mM and a component molar ratio of 7:3. The sample contains mainly small unilamellar vesicles (SUVs) with a large size distribution ranging from 20 to 250 nm in diameter. It also contains some tubules (not shown). Most of the vesicles are smooth and spherical, an indication of highly rigid bilayers. The thermal energy is thus not capable to deform the vesicles. The micrograph contains one large vesicle encapsulating smaller vesicles. The interlamellar distance between two adjacent bilayers is rather constant, about 30 nm. This is an indication that the bilayers are ionically charged and repel each other. On the basis of the 3 mM NaBr concentration that comes from the two components, the separation of 30 nm makes sense.

Figure 4B shows a vitrified cryo-TEM specimen of the turbid 8:2 solution. The micrograph shows large multilamellar vesicles of diameters up to about 1 $\mu$m, which contain up to eight concentric shells. This diameter is much larger than the thickness of the vitrified liquid film for the cryo-TEM preparation. The bilayers of the vesicles must therefore be so stiff that the vesicles cause local bulging of the thin liquid film. The interlamellar spacing between the individual bilayers varies between 10 and 100 nm, typically 50 nm, which is in the range of twice the Debye length of the diffuse double layer, which corresponds to the salt concentration in the solution. It is therefore likely that the bilayers of the vesicles carry an excess ionic charge and are stabilized by this charge.

The bilayers seem to be rather stiff. Even the vesicles outside of large MLVs are fairly spherical, and the membranes do not show local fluctuation on the 10 nm scale. The micrograph also shows a few tubules in the upper right corner. Those will be discussed later. It is noteworthy that the innermost shell of the large MLV shown in the micrograph has a diameter of about 500 nm and the interior of the MLV is completely empty of smaller shells. This is most unusual for MLVs, which are usually completely filled with vesicles and where the smallest vesicle inside has a diameter double the size of the interlamellar spacing.[21]

The 9:1 mixture also contains vesicles along with very few tubules. Figure 4C shows in this system MLVs as well as SLVs. The interlamellar distances here seem less well defined than in the 8:2 mixture.

Cryo-TEM images of the turbid solutions with a mixing ratio of 5:5 (e.g., Figure 4D) show only vesicles. No other structures have been imaged by cryo-TEM. Several special features of the vesicles are noteworthy. The micrographs contain vesicles with one to four shells. However, in contrast to the MLV of Figure 4B, there is little interlamellar spacing between the individual shells; the bilayers inside one MLV seem to touch each other (white arrow in the figure). It can therefore be concluded that there is little repulsion between the bilayers because the bilayers do not carry excess ionic charges. Because the bilayers are rather stiff, they do not exert repulsive forces due to undulation motion of the bilayers. The smallest unilamellar vesicles have a diameter of about 25 nm and are perfect spheres. Even unilamellar vesicles that are as large as 100 nm are still perfect spheres. Perfect spherical vesicles can even be observed on the support film (dark diagonal feature). It is also clear from the micrograph that the vesicles are densely packed

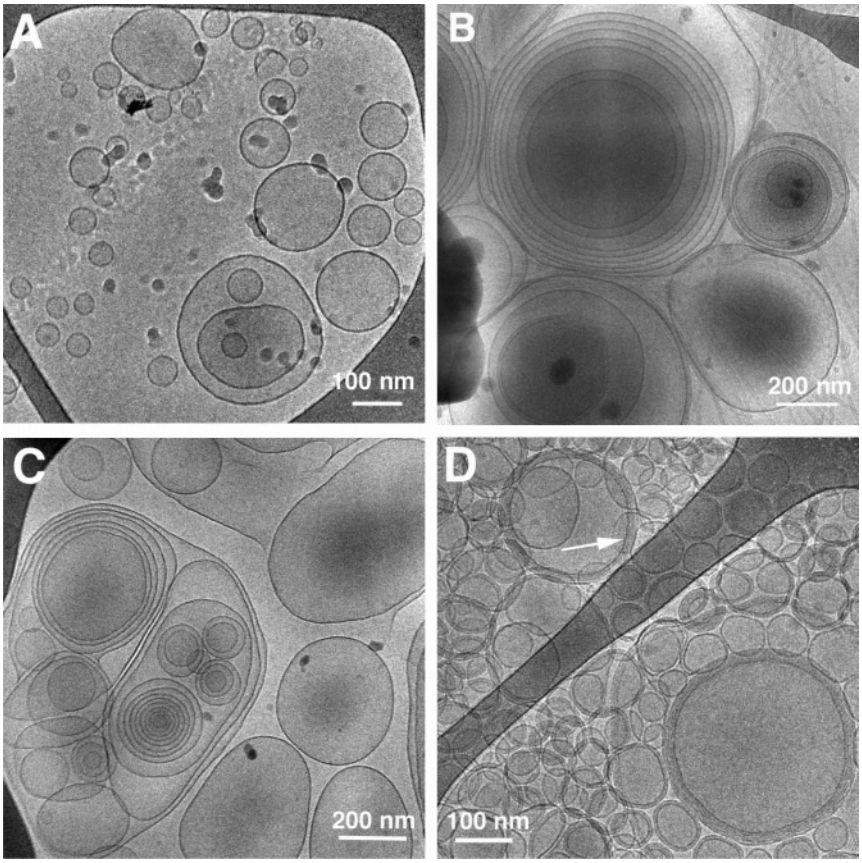


**Figure 4.** Cryo-TEM images of the PhBSA (Na salt) with CTAB system, $c^\circ = 10$ mM, at different ratios: (A) 7:3, (B) 8:2, (C) 9:1, (D) 5:5. See the text for details.

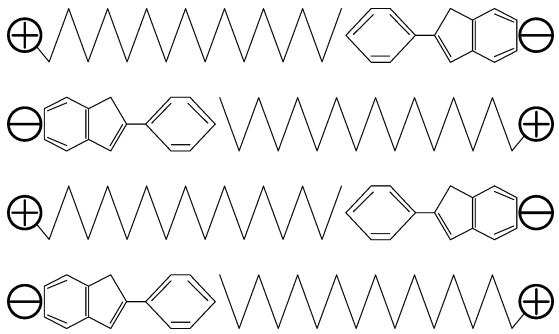

**Figure 5.** Schematic model for the interdigitated state of the bilayers.

in space, not only on top of each other. The entire shell of a vesicle with four bilayers (arrow) has a thickness of about 17 nm. This means that one bilayer is about 4 nm thick. This corresponds to the thickness that is given by the interdigitated state as shown in Figure 5.

The schematic molecular arrangement in Figure 5 explains why the bilayer is so stiff. The PhBSA molecule is a stiff molecule which cannot form kinks like the hydrocarbon chain of CTAB. This rigidity is in agreement with the spherical shape found by cryo-TEM. Thermal energy can obviously not deform these spherical vesicles to ellipsoidal vesicles. While at present micrographs are not available from each mixture of the PhBSA-rich side of the phase diagram, it is likely that all the mixtures from 9:1 to 5:5 contain the same type of vesicles. We assume that all these vesicles have the same composition as the bulk samples. It is easily conceivable that the surface of the vesicles is somewhat hydrophobic due to the methyl groups from the CTAB molecules.

In the 4:6 mixtures at the CTAB-rich side vesicles are also observed, Figure 6A. Those are very different from the vesicles on the PhBSA-rich side. All the observed vesicles have only one bilayer. The bilayer seems much more flexible. The vesicles are not spherical, and in general, they are elliptically deformed. Furthermore, the bilayers seem to have pores of the size of the thickness of the bilayer. The shown vesicles are reminiscent of "holey vesicles" which have been observed in other surfactant mixtures.[22] Some of the vesicles are attached to long threadlike micelles (arrows in Figure 6A). Similar tethering had been shown by Danino et al.[23] It is conceivable that the threadlike micelles are formed first when the components are mixed and the resulting structures are then transformed into vesicles. However, it could also be the other way around. At present the situation is not completely clear. More measurements, in particular good resolution time kinetic measurements, should be carried out.

Also on the CTAB-rich side of the phase diagram is the 3:7 mixture (Figure 6B), which behaves quite differently from all the other mixtures that have been described so far, showing threadlike structures. This system is discussed in detail later.

*Gelled State*. A cryo-TEM micrograph from this region for the mixing ratio 8:2 is shown in Figure 6C. To prepare the specimen, the gels were first "liquefied" by vigorous shaking of the vial. The resulting viscous liquid could then be made into the thin liquid film needed for cryo-TEM. All cryo-TEM images of this system, e.g., Figure 6C, show tubules of the same diameter. The outer diameter of the tubules is about $12 \pm 1$ nm, and the inside diameter is about 6 nm, independent of the mixing ratio of the samples. The tubules are many micrometers long. They are rather stiff and have a persistence length of several micrometers. The independence of the dimensions of the tubules of the mixing conditions makes it likely that the tubules have the same composition, namely, a composition of

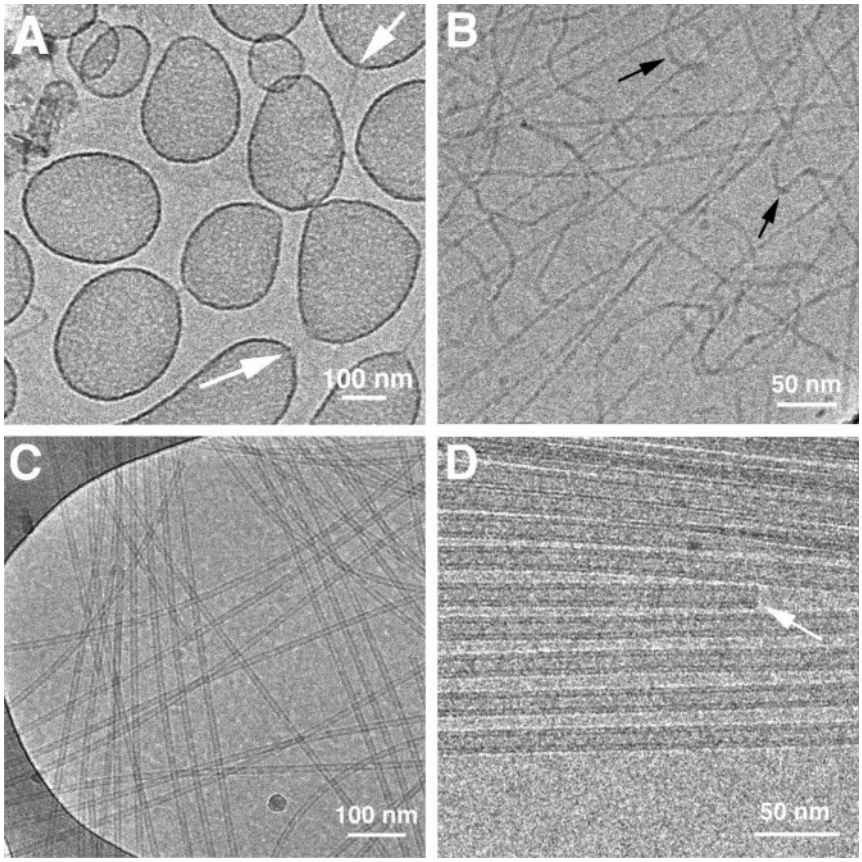


**Figure 6.** Cryo-TEM images of the PhBSA (Na salt) with CTAB system, $c^{\circ} = 20$ mM: (A, B) images of the CTAB-rich side of the phase diagram, (C, D) images of the gel phases; (A) 4:6 component mole ratio, (B) 3:7, (C) 8:2, (D) 9:1 (high-magnification image). See the text for details.

PhBSA to CTAB of 1:1. It is likely that a single tubule develops from the bilayer of one vesicle. The tubules are not connected into a three-dimensional network. The stability of the network and hence the formation of the hydrogel is simply given by the stiffness and the length of the tubules that overlap in solution and form an entangled mesh. Each tubule is locked in position by the neighboring tubules and can no longer freely diffuse. The hydrogel therefore represents a glassy state of the tubules: the solvent is kept in this network by capillary forces. For that reason the gel character of the system is lost when the tubules are broken by force. The network cannot reassemble under normal conditions.

A higher magnification of the tubules formed in the 9:1 molar ratio system is shown in Figure 6D. The inner structure of the tubule walls is clearly resolved, as manifested by the variation of electron density across the tubule diameter. Each wall is resolved into two dark lines, which may reflect higher local density. The arrow in the figure points to a rare tubule end captured in the field of view, showing that the tubules are open (not capped). Such ends are rare in the micrographs because of the tubules' lengths.

Finally, we return to the unusual 3:7 system. Upon mixing of the two components, the obtained mixture is transparent and viscoelastic. With time a sediment is formed. Micrographs from the relatively fresh samples before precipitation show long threadlike objects (Figure 6B) about 4 nm thick. The threadlike micelles (TLMs) have an extremely long persistence length of more than 1 $\mu$m, very different from the persistence length of wormlike micelles of a $C_{16}$ chain. Note that the TLMs are arranged in several different directions, excluding the possibility of stretching during specimen preparation. Close inspection of the aggregates shows that at least some of the threadlike micelles

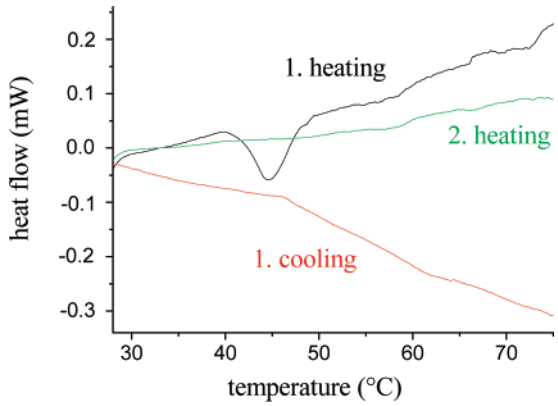


**Figure 7.** DSC data for a gelled 50 mM sample with a molar ratio of 8:2. Note that the endothermic peak occurs only during the first scan, not during the cooling scan nor in the reheating scan.

are narrow ribbons with a helical twist. Arrows point to wider segments in projection of the aggregates, characteristic of twisted narrow ribbons. It is not clear yet whether two forms of aggregates, true threadlike micelles and ribbons, coexist or whether one type is transformed into the other form with time. Such ribbons have been reported; a recent example is by Candau and co-workers.[24]

**DSC**. DSC measurements of the gelled samples were performed to determine their melting temperature and melting enthalpy as a function of the component ratio in the mixed catanionic systems. On heating, we observed a well-defined peak at around 45 °C, Figure 7. The peak occurs at the same temperature at which the gels transform into low-viscosity solutions. It is noteworthy that the melting peak appears only

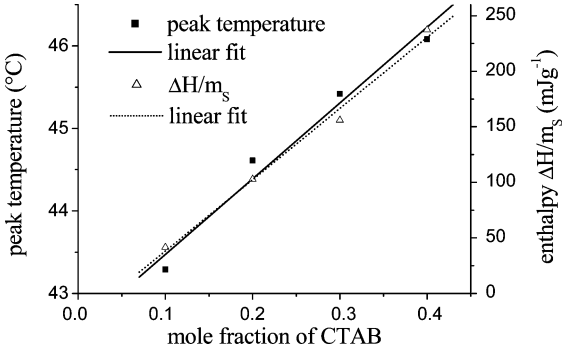


**Figure 8.** Melting temperature and the heat of melting for 50 mM solutions against the mole ratio of CTAB.

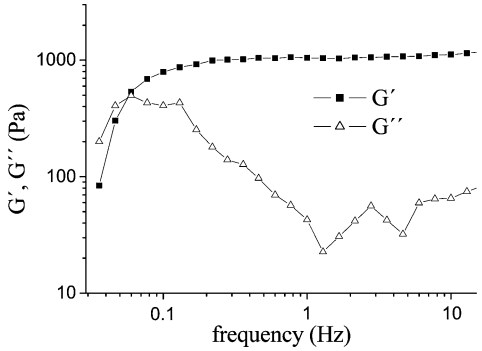


**Figure 9.** Rheogram of a sample with an 8:2 mole ratio and a total concentration of 20 mM (stress $\sigma = 0.05$ Pa, $T = 25$ °C, 7 days after mixing). Note that the storage modulus, $G'$, is about an order of magnitude higher than the loss modulus, $G''$; $G'$ is independent of frequency in most of the examined range.

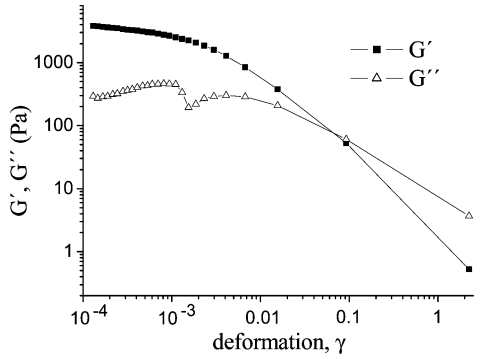


**Figure 10.** Storage and loss moduli as a function of deformation of the sample of Figure 9 at a constant frequency of 1 Hz. Note that the modulus begins to break down at a deformation of ca. 0.002.

at the first heating cycle of a gelled sample. The peak does not appear during the cooling period or on reheating. This is consistent with the observed behavior that samples can be kept below the gelling temperatures for many days before the samples become gels. The melting peak for different mixing ratios of the samples occurs roughly at the same temperature of 45 ± 1.5 °C. If the composition of the structures that cause the melting peak were the same as the bulk composition of the samples, i.e., if it would change from 9:1 to 6:4, then the melting temperatures would be expected to differ much more strongly between the samples. The crystalline or semicrystalline matter that gives rise to the DSC peak therefore must be expected to have a very similar composition in all four investigated samples, despite the huge differences in their bulk composition.

However, the heat of melting changes by about a factor of 4 when samples with the 9:1 and 6:4 ratios are heated. These results indicate that the amount of crystalline material is proportional to the CTAB content in the sample and that the crystalline material has a 1:1 composition. On close inspection, one finds that the heat of transformation and the melting temperature increase linearly with the mole fraction of CTAB (Figure 8). The simplest explanation for these results is that the two compounds form a 1:1 complex which has the highest melting temperature. In the mixtures with excess PhBSA, some excess molecules are incorporated into the crystalline bilayers, which results in lowering of the melting temperature. In comparison to the heat of melting of another catanionic compound with a $C_{16}$ chain and an aromatic counterion, namely, the compound cetyltrimethylammonium 3-hydroxy-2-naphthoate, that has a melting enthalpy of 55 kJ/mol, the heat of melting of the tubules is, at 10 kJ/mol,[25] rather low. This can be an indication that the tubules are in a semicrystalline state that is very different from a crystalline three-dimensional bulk state. It is therefore not surprising that the tubules are transformed into a real crystalline state, when they are kept at a lower temperature for longer time periods.

**Rheology**. The gel phases are the ones that we focused on in the rheological study. All the mixed samples on the PhBSA-rich side behave very similarly. Recall that low-viscosity vesicular dispersions are formed upon mixing the components; the Newtonian viscous behavior of these systems is not very interesting and was not studied in detail. With time, dependent on the mixing ratio, those samples gel. The rheological measurements of those hydrogels are reported here. The measurements were carried out on gel samples which had been prepared in the rheometer: the low-viscosity solutions were poured into the instrument and were allowed to gel. This was done to avoid destruction of the gels when transferred into the rheometer.

A typical rheogram of the 8:2 molar ratio, 20 mM total concentration sample (Figure 9) shows characteristic gel features. The storage modulus, $G'$, is about an order of magnitude larger than the loss modulus, $G''$, and frequency independent in almost the entire frequency range. The storage modulus, 1000 Pa, is rather high for a system of only 20 mM of low molecular weight components.

The yield stress can be determined from Figure 10, where the storage modulus for a constant frequency of 1 Hz is plotted as a function of deformation. In this plot the yield stress can be obtained from the critical deformation, $\gamma_c$, at which the storage modulus breaks down. The product of the storage modulus with $\gamma_c$ is the yield stress. Estimating the breakdown to occur at $\gamma = 0.002$, where $G' = 3000$ Pa, a yield stress of 6 Pa is obtained.

**SAXS**. As with the rheology, we focused our attention here on the gelled states. Typical SAXS scattering data of gelled samples are shown in Figure 11. Three of the samples contain a total concentration of 50 mM with molar ratios of the two components of 9:1, 8:2, and 7:3, and one sample had a concentration of 10 mM with a component ratio of 6:4. It is noteworthy that the three samples with a total concentration of 50 mM have about the same scattering intensity in the $q$ range between 0.5 and 1.5 $nm^{-1}$, while the sample with a concentration of 10 mM has, as one would expect, a much lower scattering intensity. In this $q$ range the scattering intensities seem to depend mainly on the total concentration, not so much on the component ratio. This is contrary to the DSC results which showed that the melting peak for the samples depended on the mixing ratio and increased linearly with the CTAB concentration. Thus, the SAXS data indicate qualitatively that the structures that give the scattering curves contain the total amount of both compo-

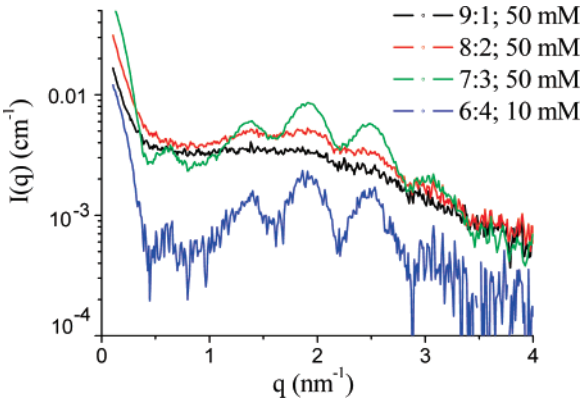


**Figure 11.** SAXS data for four different PhBSA (Na salt)/CTAB mixtures. Note that the scattering intensities for the solutions with the same total concentration, but different mole ratios, are about the same. The $q$ values for all corresponding peaks are about the same.

nents, not only the amount that forms the semicrystalline tubules. Such a conclusion would be in agreement with the NMR data.

At $q$ values that are larger than 1.5 $nm^{-1}$ the three scattering curves for the 50 mM samples deviate from one to the other. With increasing CTAB concentration the scattering curves show oscillations with the scattering vector $q$. The oscillations are most expressed for the 50 mM 7:3 sample and also for the 10 mM 6:4 sample. The oscillations are typical for monodisperse tubules with a radially symmetric cross-section. The lack of these oscillations can have different reasons, which are not easy to distinguish via scattering methods. The cylinders can be polydisperse in their size, but they can also be polydisperse in the shape of the cross-section; i.e., they may deviate from circular symmetry. Another reason could be that some cylinders stick together. Again, the form of the cross-section of such an aggregate would then deviate from a simple circular one.

Within accuracy of the scattering data, the scattering maxima and minima of the oscillation for the different mixtures occur at the same position. This is an indication that the cross-section dimensions of the tubules are independent of the mixing ratio of the solutions. Remember that the tubule images by cryo-TEM all look the same at different concentrations and mixing ratios, while the scattering curves for different samples are significantly different. Hence, the scattering curves contain details that cannot be recognized by cryo-TEM. The most obvious parameter of the tubules that varies with composition is the polydispersity or deviation from radial symmetry. It becomes smaller when the mole ratio of the components approaches 5:5.

The scattering intensities from samples with the same composition, but of different total concentration, increase linearly with the concentration, as expected, independently of the $q$ values (data not shown). The positions of the side maxima remain unchanged; thus, the cross-section of the tubules does not change with the overall concentration. However, these side maxima are less pronounced with higher concentration. A possible explanation could be the higher amount of adsorbed free excess molecules.

To determine the dimensions of the tubule cross-section, we calculated the pair distance distribution functions (PDDFs) from the scattering functions, using the IFT method. The radial difference electron density profile $\Delta\rho(r)$ of the cross-section of the cylinder was finely obtained by deconvolution of $p_c(r)$ (Figure 12). It gives a clear indication of a hollow cylinder with a bilayer wall. On the basis of these data, the evaluated dimensions of the tubules are inner radius 3.5 nm, total wall

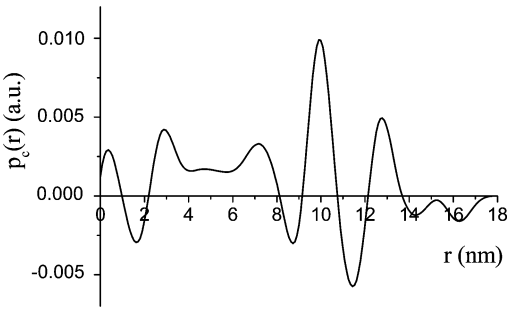


**Figure 12.** Pair distance distribution function for a 50 mM solution and a mole ratio of 7:3. Electron density of the tubules in the 50 mM solution with a mole ratio of 7:3 as a function of the distance from the cylinder axis. The horizontal and dotted line at a value of 0.0 corresponds to the level of the electron density of the solvent.

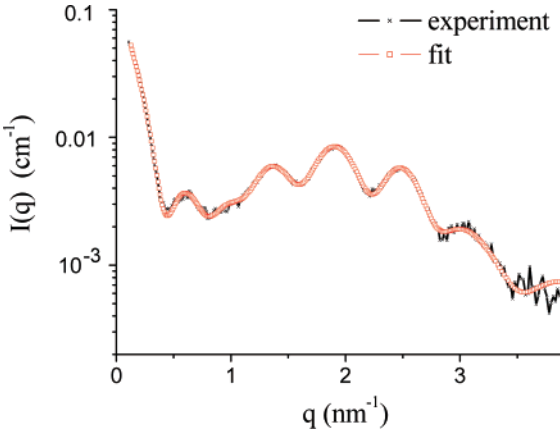


**Figure 13.** Comparison of the experimental scattering function with the IFT-fit function for a 50 mM sample of a 7:3 mole ratio.

thickness 3.5 nm, inner palisade layer thickness 1 nm, hydrophobic core thickness 1.5 nm, outer palisade layer thickness 1 nm, and outer tubule diameter 14 nm.

The results indicate that the outer diameter of the tubules as determined from the SAXS data is about 1 nm larger than the diameter determined from the cryo-TEM measurements. This is a reasonable agreement, as one has to take into consideration the inaccuracies of the TEM magnification, errors due to defocus, and measurement inaccuracies. Cryo-TEM is an excellent tool for the identification of the building blocks of the structures, but quantification is much more accurate with other, nonimaging ("indirect") techniques, such as SAXS. However, SAXS can give no information on the overall length or stiffness of the tubules; i.e., the two methods give complementary information.

In Figure 13, we show a comparison of an experimental scattering function with the IFT fit function. The experimental curve is matched in all details by the fitted function.

## Conclusions

We have shown that aqueous mixtures of the stiff anionic compound PhBSA and the cationic surfactant CTAB have a rich and time-dependent phase behavior. Multilamellar vesicles are formed immediately upon mixing samples of the two compounds at an excess of PhBSA; those are stable for many days. Then, within 1 day, the low-viscosity, somewhat turbid vesicle phases are transformed into clear hydrogels. On a molecular level the gelation of the sample is caused by a transformation of the vesicles into many micrometers long stiff nanotubules with a very small diameter of 14 nm, as determined by cryo-TEM and SAXS. Rheological measurements show that

the hydrogel phase has the characteristics of a typical gel phase. DSC has shown that each composition has a characteristic melting temperature. The tubules themselves have a 1:1 molar ratio of the two components. The excess PhBSA seems to be adsorbed on the tubules. Upon longer aging many of these systems form crystalline precipitates. On the CTAB-rich side, the mixtures are clear viscoelastic solutions of threadlike and ribbonlike structures that do not change with time.

## References and Notes

(1) Schwarz, U. S.; Safran, S. A. *Phys. Rev. E* **2000**, *62* (5), 6957.
(2) Harutyunyan, A. R.; Pradhan, B. K.; Kim, U. J.; Chen, G.; Eklund, P. C. *Nano Lett.* **2002**, *2*, 525−530.
(3) Terech, P.; Talmon, Y. *Langmuir* **2002**, *18*, 7240−7244.
(4) Schnur, J. M. *Science* **1993**, *262*, 1669.
(5) Shimizu, T.; Masuda, M.; Minamikawa, H. *Chem. Rev.* **2005**, *105*, 1401−1443.
(6) Imae, T.; Funayama, K.; Kraft, M. P.; Giulieri, F.; Tada, T.; Matsumoto, T. *J. Colloid Interface Sci.* **1999**, *212*, 330−337.
(7) Ohta, A.; Danev, R.; Nagayama, K.; Mita, T.; Asakawa, T.; Miyagishi, S. *Langmuir* **2006**, *22*, 8472−8477.
(8) Evans, E.; Bowman, H.; Leung, A.; Needham, D.; Tirrell, D. *Science* **1996**, *273*, 933.
(9) Zhai, L.; Herzog, B.; Drechsler, M.; Hoffmann, H. *J. Phys. Chem. B* **2006**, *110*, 36.
(10) Kaler, E. W.; Murthy, A. K.; Rodrigues, B. E.; Zasadzinski, J. A. N. *Science* **1989**, *245*, 1371.
(11) Hao, J.; Hoffmann, H.; Horbaschek, K. *Langmuir* **2001**, *17*, 4151−4160.
(12) Pakk, Y.; Blankschtein, D. *Langmuir* **1996**, *12*, 3802−3818.
(13) Hao, J.; Liu, W.; Xu, G.; Zheng, L.; Hoffmann, H. *Langmuir* **2003**, *19*, 10635−10640.
(14) Talmon, Y. In *Giant Micelles*; Zana, R., Kaler, E. W., Eds.; CRC Press: New York, 2007; pp 163−178.
(15) Glatter, O. *J. Appl. Crystallogr.* **1977**, *10*, 415−421.
(16) Glatter, O. *Small Angle X-Ray Scattering*; Academic Press: London, 1982; pp 119−165.
(17) Glatter, O. *J. Appl. Crystallogr.* **1980**, *13*, 577−584.
(18) Glatter, O.; Hainisch, B. *J. Appl. Crystallogr.* **1984**, *17*, 435−441.
(19) Glatter, O. *Prog. Colloid Polym. Sci.* **1991**, *84*, 46−54.
(20) Hoffmann, H. Tubules from a stiff anionic counter-ion and alkyltrimethylammonium ions: The influence of the chainlength. Manuscript in preparation.
(21) Hao, J.; Hoffmann, H.; Horbaschek, K. *J. Phys. Chem. B* **2000**, *104*, 10144−10153.
(22) Edwards, K.; Gustafsson, J.; Almgren, M.; Karlsson, G. *J. Colloid Interface Sci.* **1993**, *161*, 299.
(23) Danino, D.; Bernheim-Groswasser, A.; Talmon, Y. *Colloids Surf., A* **2001**, *183−185*, 113−122.
(24) Buhler, E.; Oelschlaeger, C.; Waton, G.; Rawiso, M.; Schmidt, J.; Talmon, Y.; Candau, J. *Langmuir* **2006**, *22*, 2534−2542.
(25) Horbaschek, K.; Hoffmann, H.; Thunig, C. *J. Colloid Interface Sci.* **1998**, *206*, 439−456.
(26) Jing, L.; Hoffmann, H. *Colloid Polym. Sci.* **2004**, *283*, 24−32.